Dynamic response of a quantum point contact

C. Karadi, S. Jauhar, L. P. Kouwenhoven, K. Wald, J. Orenstein, and P. L. McEuen

Department of Physics, University of California, Berkeley, and Materials Science Division, Lawrence Berkeley Laboratory, Mail Stop 2-300, Berkeley, California 94720

Y. Nagamune and H. Sakaki*

Research Center for Advanced Science and Technology, University of Tokyo, 4-6-1 Komaba, Meguro-ku, Tokyo 153, Japan

Received March 10, 1994; revised manuscript received July 5, 1994

We report measurements of the dc current ΔI_{dc} generated across a nanometer-scale constriction, or a quantum point contact (QPC), in the two-dimensional electron gas in the GaAs–GaAlAs system. ΔI_{dc} was induced by photoexcitation of the QPC in the terahertz regime. To our knowledge, these are the first measurements in which the induced current has been measured as a function of the excitation frequency ω. Spectra of ΔI_{dc} versus ω were obtained with a time-domain interferometer based on photoconductive (Auston) switch sources of pulsed terahertz radiation. The pulses were coupled to the gate that defines the QPC by a combination of quasi-optical techniques and a novel antenna–transmission-line structure. The spectra are a strong function of the height of the barrier that creates the constriction, which suggests that photon-assisted transport is a possible mechanism for the induced dc current. Measurements of the QPC response demonstrate the applicability of this technique to a variety of other mesoscopic structures, such as single and multiple quantum dots.

INTRODUCTION

Extensive studies of electronic transport in the quantum regime have led to a deep understanding of the near-zero frequency conductance of mesoscopic structures. In contrast, our understanding of the high-frequency response is much less well developed partially because of the comparative lack of experimental results. Recently several theoretical studies on the nonlinear response[1–4] and the linear response[5–7] of mesoscopic devices have appeared, increasing researchers' motivation to conduct more experiments. In this paper we describe a novel technique for probing the high-frequency properties of the simplest of the mesoscopic structures, the quantum point contact (QPC). This technique can be extended to other mesoscopic devices, and measurements on quantum dots are in progress.[8]

A QPC is a constriction whose size is of the order of the Fermi wavelength, separating two metallic regions. The most studied example, and the one that we have used, is a QPC implemented in the two-dimensional electron gas (2DEG) at a GaAs–GaAlAs heterojunction.[9,10] Typically the constriction is formed by a split metallic gate electrode deposited on the surface, approximately 100 nm above the 2DEG. The QPC in the 2DEG is an elegant realization of low-dimensional electronic transport with a voltage-tunable barrier.

In our experiments we are interested in the dc current that flows across the constriction in response to ac excitation in the terahertz regime. The generation of a rectified current ΔI_{dc} requires some asymmetry in the structure, either built in or imposed by a dc bias voltage. As we explain below, in our devices it appears that ΔI_{dc} is most strongly influenced by an asymmetry built into the structure.

Our motivation for studying rectification in a QPC stems from several sources. The ability to couple high-frequency radiation to the QPC is an essential prerequisite for terahertz spectroscopy of more complicated mesoscopic structures. For example, we hope to perform spectroscopic measurements on confined electronic systems, such as quantum dots. In the GaAs–GaAlAs system quantum dots are fabricated with gate electrodes, and transport in and out of the dot occurs by means of QPC's with voltage-tunable conductance. Characterization of the rectified current through a QPC tests whether we can efficiently couple terahertz radiation to the QPC. Most importantly, we need to know if the current generated in response to the high-frequency excitation is coherent with the ac field or whether it derives from incoherent local heating of the electron gas.

Although a single QPC does not induce complete confinement, as in a dot, the dependence of the rectified current on the excitation frequency may still show nontrivial effects. If the width of the conductance onset as a function of barrier height is sufficiently sharp compared with $\hbar\omega$ we will access the quantum regime of photon-assisted transport. In this regime we expect that the rectified current should increase with increasing excitation frequency because higher-energy photons are more efficient in exciting electrons over the barrier. Indeed, observation of this effect would be the clearest indication that the induced currents are coherent, rather than bolometric, in origin.

TERAHERTZ SPECTROMETER

Measuring ΔI_{dc} as a function of the excitation frequency ω would be conceptually simplest with the use of a tunable continuous-wave (cw) source to provide the excitation. Unfortunately such sources are difficult to obtain in the

0740-3224/94/122566-06$06.00

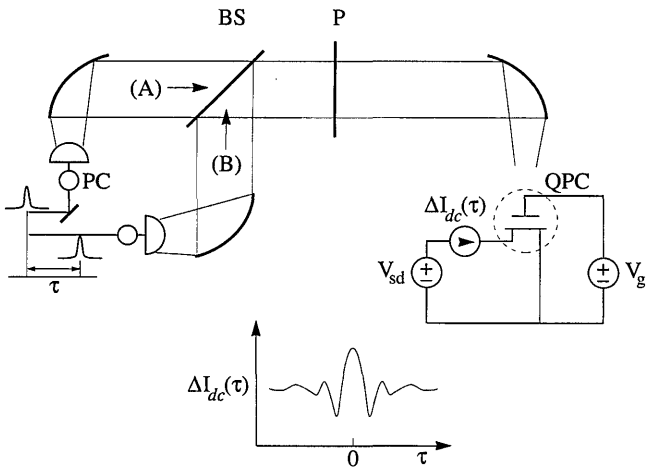

Fig. 1. Schematic diagram of the time-domain interferometer. BS, wire-grid beam splitter; P, wire-grid polarizer; PC, photoconductive Auston switch.

millimeter range of the spectrum. Two groups have studied ΔI_{dc} in a QPC with a single-frequency source, either a far-infrared molecular laser[11] or a Gunn oscillator.[12] The measurements of Wyss *et al.*[12] demonstrate that it is difficult to distinguish a coherent from a bolometric response based on measurements at a single frequency.

To measure the frequency dependence of the rectified current we use a recently developed technique based on a pulsed rather than a cw source. Greene *et al.*[13] devised a time-domain interferometer to characterize the spectrum of terahertz pulses generated by optical excitation of a semi-insulating InP wafer. A bolometer served as a square-law detector with a flat frequency response throughout the terahertz regime. By replacement of the bolometer with a device under test, the same technique becomes a spectroscopic tool. Using a spectrometer of this type, we performed the first, to our knowledge, broadband measurements of a superconductor–insulator–superconductor millimeter-wave detector.[14]

Figure 1 shows a diagram of the spectrometer. The pulsed source is a photoconductive Auston switch[15] coupled to a 300-μm dipole antenna,[16] which radiates when excited with a mode-locked Ti:sapphire laser. The emitted pulse is nearly a single cycle of the electric field, with an approximate period of 5 ps. The power spectrum of the pulse has a center frequency of 180 GHz and a 3-dB bandwidth of 80 GHz. To study ΔI_{dc} versus ω we measure the dc current induced by two pulse trains as a function of their relative arrival time τ. As depicted schematically in Fig. 1, we form the two-pulse beam by combining the radiation from a pair of antennas, using a wire-grid beam splitter.

The wire grid has a number of advantages over an earlier version of the spectrometer, which employed a Mylar beam splitter.[14] The most significant advantage is less frequency dependence of the reflection and the transmission coefficients, which is important for broadband measurements. In addition, the ideal throughput of the interferometer increases from 50% for the reflection beam splitter to 100% for the polarizing beam splitter. The configuration of the polarizers for achievement of optimum coupling is as follows: the two antennas are aligned at 45° with respect to the horizontal. The axis of the beam splitter is adjusted to transmit the pulse from (A) and to reflect the pulse from (B) (see Fig. 1). The combined beam contains two pulse trains with orthogonal polarizations. An additional polarizer (P) between the beam splitter and the sample selects either horizontal or vertical polarization for excitation of the device.

An f#3 parabolic mirror focuses the combined beam onto the sample through a number of windows in a ^{3}He, 7-T magnet cryostat. The beam first passes through a 25-μm Mylar room-temperature window followed by two cold quartz windows, one at 77 K and the other at 4.2 K. These windows, of thickness 6 and 9 mm, respectively, are required for blocking thermal radiation and allow the sample to reach a base temperature of 0.5 K. The beam finally enters the sample cell through a 125-μm Mylar window. The use of windows that are either much thinner or much thicker than the pulse length eliminates reflections that might otherwise contaminate the signal. The sample rests immersed in superfluid ^{3}He. The superfluid is quiescent, eliminating the possibility of bubbles' causing instabilities in the device and in beam propagation.

ANTENNA–TRANSMISSION-LINE COUPLING

Figure 2 shows our scheme for coupling terahertz radiation to the QPC device. Our technique ensures that ac potentials are applied to the QPC in a controlled manner. The antenna–transmission-line chip and the QPC chip are both mounted in a standard 16-pin carrier (not shown). The chip carrier is secured to a brass plate, which prevents terahertz radiation from falling directly on the device. To reach the QPC, incident radiation from below must first pass through a small hole in the brass plate fitted with a 4-mm-diameter hyperhemispherical Si lens. The Si lens focuses the beam onto a 600-μm dipole antenna designed to resonate at approximately 90 GHz. Because of the wide bandwidth of dipole antennas, substantial overlap remains between the picosecond pulses centered at 180 GHz and the receiving antenna centered at 90 GHz. The advantage of this design is that the power coupled to the antenna will be relatively evenly

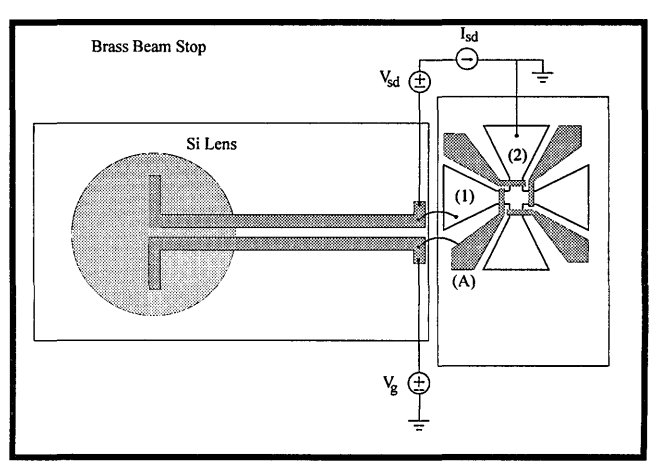

Fig. 2. Schematic diagram of the antenna–transmission-line coupling to the QPC device.

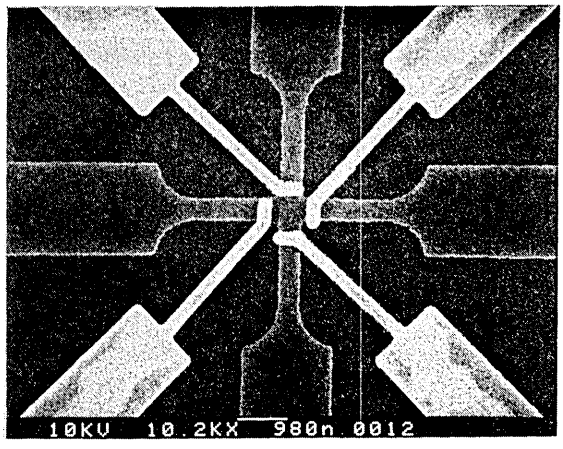

Fig. 3. Scanning electron micrograph of the QPC device.

distributed from 90 to 180 GHz. From the antenna the pulses are coupled to an impedance-matched 5-mm-long coplanar transmission line. Both the antenna and the transmission line consist of 0.8-μm-thick Al evaporated onto a 0.5-mm-thick sapphire substrate. Once the pulse reaches the end of the transmission line on the antenna chip it hops onto the QPC chip via 100-μm-long gold wire bonds.

DEVICE UNDER STUDY

The QPC that we studied differs somewhat from the split-gate version. Figure 3 shows a scanning electron micrograph of the device[17] used in our experiments. In the region of interest two narrow channels of 2DEG, of 460-nm width, intersect to form a cross. Because of depletion of electrons at the edges the effective channel width is reduced to nearly 60 nm. The narrow wires eventually grow into millimeter-wide 2DEG regions characterized by a mobility of 800,000 $cm^2/V\,s$ at 4.2 K and a density of 2.0×10^{11} cm^{-2}.

In contrast to the split-gate QPC, each channel of our device has a gate that overlaps its entire width. Application of a negative voltage to a gate generates a barrier for electron propagation. With four gates the structure may be configured for a wide variety of experiments, including the demonstration of Coulomb blockade oscillations and turnstile operation.[17] To date, we have studied the high-frequency response of the device with only one gate active, forming a QPC. In the future, activating all four gates will allow us to study the high-frequency response of a quantum dot.

DIRECT-CURRENT TRANSPORT

As shown in Fig. 2, the high-frequency voltage is applied to the QPC via gate (A) and ohmic contact (1). In addition to receiving the ac input from the transmission line, the QPC is biased (typically at 100 μV) through source and drain ohmic contacts (1) and (2). A negative voltage applied to the gate creates a tunable barrier.

The solid curve shown in Fig. 4(a) shows a typical trace of the dc current that flows from source to drain I_{sd}, as a function of the gate voltage V_g, for an applied bias V_{sd} of 100 μV. There is a sharp increase in conductance when $-V_g$ drops below approximately 750 mV. The curves of I_{sd} versus V_g near the onset of conductance differ from device to device, and the same device will have different behavior depending on the history of temperature cycling and of visible-light exposure. In general, these devices do not exhibit the quantized conductance steps of size $2e^2/h$ seen in QPC's formed by split gates.[9,10] We believe that electron backscattering in the channel, which leads to a breakdown of the conductance quantization, is the reason for the absence of conductance steps. The steps

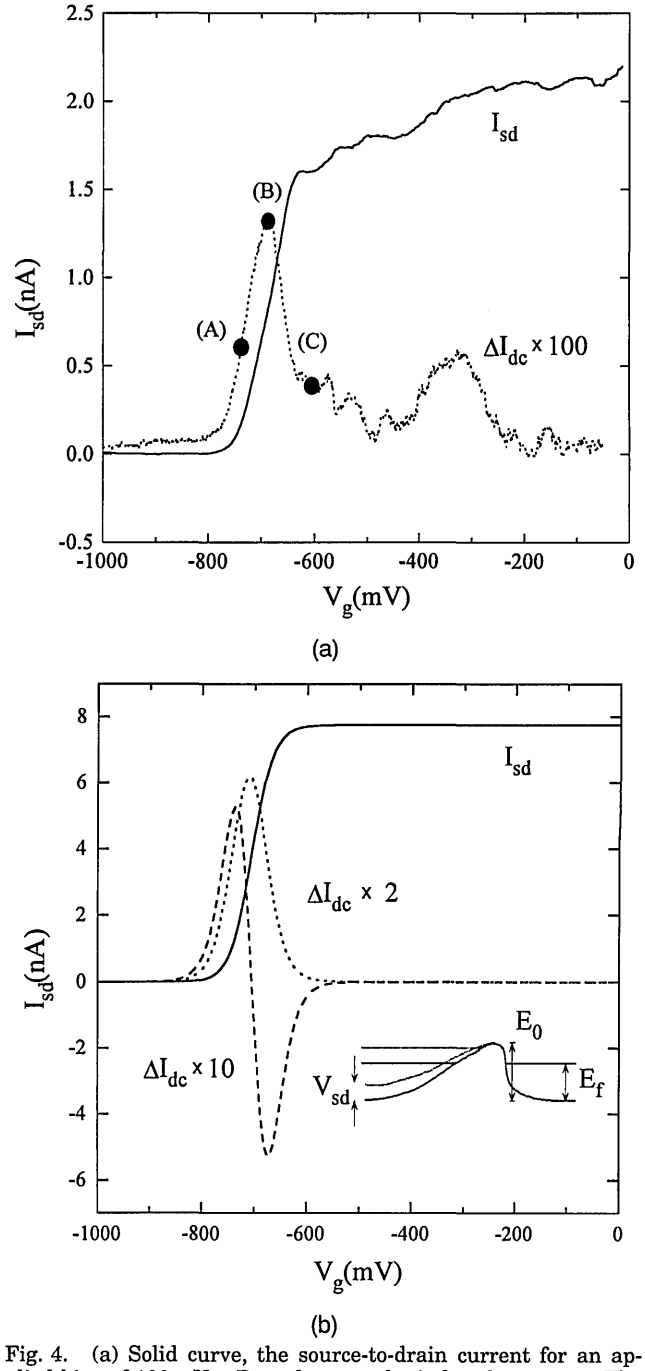

Fig. 4. (a) Solid curve, the source-to-drain current for an applied bias of 100 μV. Dotted curve, the induced current. The cross correlations at points (A)–(C) are shown in Fig. 5. (b) Solid curve, a model calculation of the source-to-drain current versus the gate voltage for an asymmetric barrier (inset). Dotted curve, the calculated induced current for V_{sd} replaced by $V_{sd} + V_{ac}\sin(\omega t)$. Dashed curve, the calculated induced current for sinusoidal variation of the barrier height E_0.

are recovered on application of a small magnetic field that reduces backscattering within the channel.

SINGLE-PULSE EXPERIMENT

Before considering the interferometric response, we discuss the rectified current created by individual voltage pulses. We define the induced current ΔI_{dc} as the additional dc current that flows from source to drain when the device is irradiated with a train of pulses. To measure ΔI_{dc}, the laser beam that generates the terahertz pulses is mechanically chopped at 100 Hz, and the synchronous source-to-drain current is detected with a lock-in amplifier.

The dashed curve in Fig. 4(a) shows ΔI_{dc} versus V_g under the same experimental conditions as are given for the solid curve of I_{sd} versus V_g. There is a sharp increase in the induced current near the value of V_g, at which the channel becomes conducting. The induced current is localized to the region near the onset of conductance with little induced current at zero gate voltage. In addition, there is an induced current signal at $V_g \approx -300$ mV. This signal is also due to a small step in the conductance at $V_g \approx -300$ mV. For the purposes of this paper we confine our discussion to the induced current peak at $V_g \approx -700$ mV.

An important feature of Fig. 4(a) is that the curve of ΔI_{dc} versus V_g is unipolar. To understand the origin of the unipolarity, we calculate I_{sd} and ΔI_{dc} from a highly simplified, one-dimensional model. We use the Landauer formula to obtain I_{sd} and extend the same formalism to determine the dynamic response ΔI_{dc}; this calculation is known as the quasi-static approximation. We describe the regime of applicability of this approximation when we discuss the frequency dependence of ΔI_{dc}.

To account for the shape of ΔI_{dc} versus V_g the total potential U, as a function of position x, must break inversion symmetry. $U(x)$ is the sum of the barrier potential $U_0(x)$, the dc bias potential $V_{sd}(x)$, and the ac potential $V_{ac}(x)$. From measurements of I_{sd} versus V_{sd} performed on many samples, we find that $U_0(x)$ is indeed invariably asymmetric. Below we assume that this property is the dominant source of unipolarity.

For a single electronic mode the zero-temperature dc current that flows across the barrier in response to V_{sd} is given by[18–20]

$$I_{sd}[U(x), V_{sd}] = \frac{2e}{h} \int_{E_f}^{E_f + eV_{sd}} T[E, U(x)]\,dE, \qquad (1)$$

where E is the electron energy, E_f is the Fermi energy, and $T[E, U(x)]$ is the probability of transmission across the barrier. To illustrate clearly the effect of barrier asymmetry we consider an extreme case, a sawtooth barrier of the type shown in the inset in Fig. 4(b). For this barrier it is a reasonable approximation that T depends only on $E_0 - E$, the difference between the peak of the barrier potential energy and the electron energy. Specifically, we assume that T has the form of a unit step with a width Δ, i.e.,

$$T[E, U(x)] = \frac{1}{1 + \exp[(E_0 - E)/\Delta]}. \qquad (2)$$

To obtain I_{sd} versus V_g we assume, again for simplicity, that E_0 depends linearly on the gate voltage. The solid curve in Fig. 4(b) shows I_{sd} versus V_g calculated from Eq. (1), with $E_0 = e|V_g|/100$,[21] $E_f = 7$ meV, $V_{sd} = 100$ μV, and Δ set to 200 μeV. With these parameters the calculation strongly resembles the experimental data shown in Fig. 4(a).

To calculate ΔI_{dc} versus V_g we assume that the ac excitation leads to an oscillating V_{sd}. In the quasi-static limit we simply replace V_{sd} in the upper limit of the integral in Eq. (1) by $V_{sd}(t) = V_{sd} + V_{ac}\sin(\omega t)$ and average the resulting expression over one period, $2\pi/\omega$. The dotted curve in Fig. 4(b) shows ΔI_{dc} for $V_{sd} = 100$ μV and $V_{ac} = 400$ μV. The induced current calculated from the model displays the characteristic features that can be seen in the experiment; it is unipolar and is localized near the onset of dc conductance. For comparison, if ac excitation modulates only the barrier energy E_0 and not V_{sd}, a bipolar induced current is obtained. The dashed curve in Fig. 4(b) shows ΔI_{dc} for an oscillation of E_0 of 400-μeV amplitude, with V_{sd} fixed at 100 μV.

Note that the agreement between theory and experiment for ΔI_{dc} versus V_g addresses only the origin of the unipolarity and does not demonstrate the validity of the quasi-static approximation. Once unipolarity is established by the asymmetry the remaining feature to be fitted is the width of the peak in ΔI_{dc} versus V_g. In the quasi-static limit this feature is controlled by the width of the conductance step and the amplitude V_{ac} of the V_{sd} oscillations. The quasi-static approximation breaks down when $\hbar\omega \geq \Delta$. In this regime the width of the peak in ΔI_{dc} versus V_g is controlled instead by the energy scale of the photons in the incident pulse. For a typical frequency of 150 GHz this value corresponds to a photon energy of 625 μeV. In our experiment the typical photon energies, eV_{ac}, and Δ are all comparable, and it is extremely difficult to test the quasi-static approximation by single-pulse measurements alone. In the next section we describe spectrally resolved measurements that use two pulses.

TWO-PULSE EXPERIMENT

The magnitude of the induced current by a single pulse is an average over the response to frequencies spanned by the pulse. As mentioned above, to determine the response versus the frequency we must measure the current generated by two pulses as a function of their relative arrival time τ. This statement requires justification. To understand the connection between the τ-dependent part of the induced current $\Delta I_{dc}(\tau)$ and the frequency response $\Delta I_{dc}(\omega)$, it is useful to model the QPC as a nonlinear circuit element, in which the current generated by a time-varying voltage may be expanded in the form

$$I_{sd}(t) = \int_{-\infty}^{t} dt_1 Y^{(1)}(t - t_1)V(t_1) + \int_{-\infty}^{t} dt_1 \int_{-\infty}^{t_1} dt_2 \times Y^{(2)}(t - t_1, t - t_2)V(t_1)V(t_2) + \ldots, \qquad (3)$$

where $Y^{(n)}(t - t_1, \ldots)$ are nonlinear admittances in the time domain. For a symmetric barrier $Y^{(n)}$ vanishes for even values of n, so that there is no rectification or even-harmonic generation. Rectification occurs if the symmetry is broken by an applied bias or by an asymmetric

barrier. $Y^{(2)}$ dominates the nonlinear response for sufficiently small ac voltage. From Eq. (3) the τ-dependent part of the dc current generated by two pulses, $V_A(t)$ and $V_B(t-\tau)$, is given by[22]

$$\Delta I_{\mathrm{dc}}(\tau) = \left\langle \int \mathrm{d}t_1 \mathrm{d}t_2 G^{(2)}(t-t_1, t-t_2) V_A(t_1) V_B(t_2-\tau) \right\rangle_t , \tag{4}$$

where $G^{(2)}$, the second-order conductance, is the real part of $Y^{(2)}$. Fourier transformation of both sides of Eq. (4) with respect to τ yields

$$\Delta I_{\mathrm{dc}}(\omega) = C_{AB}(\omega) G^{(2)}(0;\ \omega, -\omega), \tag{5}$$

where $C_{AB}(\omega)$ is the Fourier transform of the cross correlation of $V_A(t)$ and $V_B(t)$. If the latter are the voltages that actually couple to the sample, then $C_{AB}(\omega)$ reflects both the spectral content of the source and the frequency-dependent coupling from free space to the QPC. The product of $C_{AB}(\omega)$ and $G^{(2)}(0;\ \omega, -\omega)$ is precisely the response function that would be obtained by measurement of the induced current versus the frequency with a tunable cw source.

Figure 5 shows $\Delta I_{\mathrm{dc}}(\tau)$ and the corresponding $\Delta I_{\mathrm{dc}}(\omega)$ for three representative values of gate voltage. The labels (A), (B), and (C) refer to the three gate voltages indicated in Fig. 4(a), respectively. The apodization function $1 + \cos(x)$ was applied to the time-domain trace to remove spurious effects in the Fourier transform that were due to truncation.[23]

Variation in the response at different gate voltages is most clearly seen in the frequency-domain data. At the peak of the response [curve (B)] the spectrum is relatively flat in the range from ≈100 to 200 GHz. The trio of resonances at 125, 160, and 190 GHz is most likely due to reflections between the QPC gate and the bonding wires. In addition, there is a peak at low frequencies ≈25 GHz. Increasing V_g so as to make the QPC more conducting leads to a spectrum [curve (C)] that cuts off sharply below ≈130 GHz. When the channel is made less conducting [curve (A)] the response spectrum is similar to curve (B). However, there is a small enhancement in the 150–200-GHz range relative to the low-frequency response at 110 GHz.

This measurement was repeated a number of times after thermal cycling of the sample, and the spectra were found to be highly reproducible. The sharp drop in the response from 75 to 130 GHz in going from curve (B) to curve (C) is especially robust. In some runs curve (A) showed a stronger enhancement of the response in the range from 150 to 200 GHz relative to the response at 110 GHz than the example given in Fig. 5. In contrast to the broadband response, the peak at 25 GHz did change dramatically on thermal cycling. In some experiments the amplitude of this peak grew to ten times the strength of the response at 150 GHz. Recent measurements of the peak position in frequency as a function of magnetic field indicate that this low-frequency peak is a plasmon in the bulk millimeter-size leads of the QPC. The variation in the peak amplitude may be attributed to variations in the electron density of the 2DEG on thermal cycling, an effect verified by Shubnikov–de Haas measurements.

The spectral changes shown in Fig. 5 indicate, in the notation of Eq. (5), that either $C_{AB}(\omega)$ or $G^{(2)}(0;\ \omega, -\omega)$ is a function of V_g. The more interesting case is variation of $G^{(2)}(0;\ \omega, -\omega)$, which would indicate a breakdown of the (frequency-independent) quasi-static approximation. This approximation breaks down when excitation frequencies comparable with, or greater than, the width of the conductance onset are achieved. In this regime the transport must be treated semiclassically, as in the Tien–Gordon theory[24] of photon-assisted tunneling. This theory predicts a suppression of $G^{(2)}(0;\ \omega, -\omega)$ for $\hbar\omega < |E_0 - E_f|$, which is a possible explanation for the low-frequency cutoff behavior shown in Fig. 5. If the

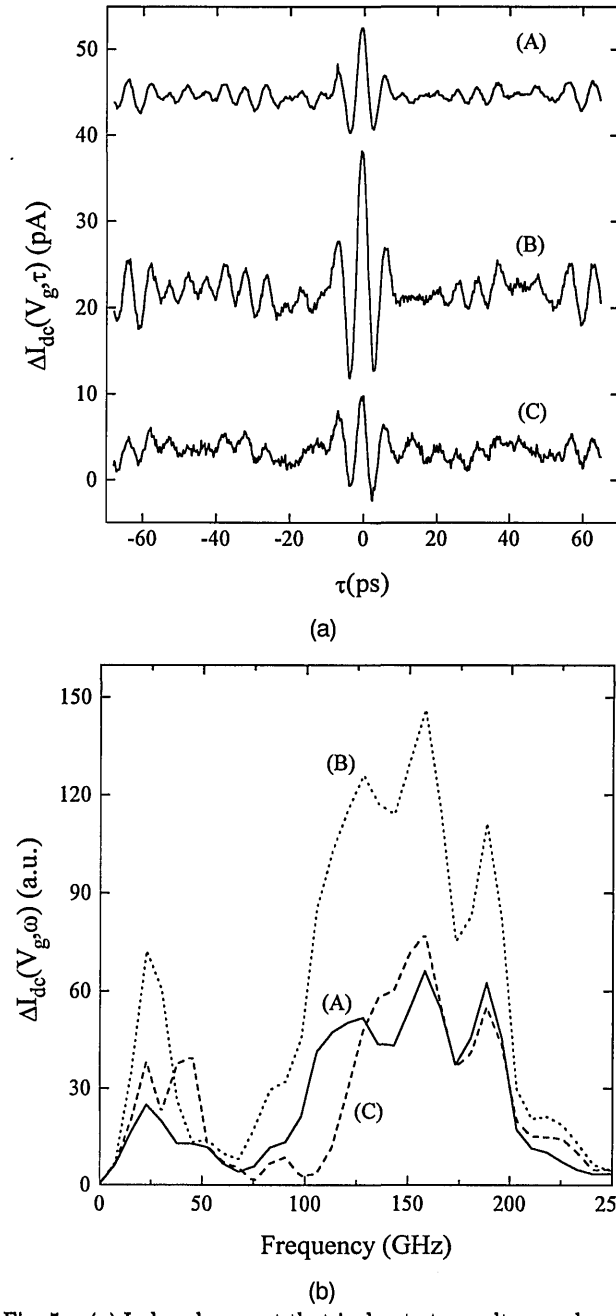

Fig. 5. (a) Induced current that is due to two voltage pulses as a function of time delay between them. Each trace is taken at a fixed gate voltage, as depicted in Fig. 4(a). Curves (A) and (B) have been offset by 10 and 40 pA, respectively. (b) Magnitude of the Fourier transforms of the interferograms shown in Fig. 5(a).

gate-voltage dependence could, in fact, be explained in this way, then local heating could be ruled out as the origin of the induced current.

Another possible explanation for the frequency dependence is that the coupling of radiation to the device, embodied in $C_{AB}(\omega)$, depends on V_g because of the corresponding changes in the barrier conductance. Testing this explanation requires modeling $C_{AB}(\omega, V_g)$; we are working to develop an equivalent circuit that includes the impedance of the bulk of the electron gas, the barrier, and parasitic reactances that are due to the gates.

CONCLUSION

We have presented what are to our knowledge the first spectra of the rectified current versus frequency in a QPC. The spectroscopic technique is general and may be applied to a variety of multiterminal mesoscopic devices. The antenna–transmission-line coupling allows us to excite well-defined terminals of the device. In future experiments the transmission-line–antenna chip will be integrated onto the device to permit the use of higher frequencies and to enhance the coupling efficiency. The frequency-dependent coupling may be measured directly by replacement of the device under test with a broadband bolometer. This successful demonstration of terahertz spectroscopy with a time-domain interferometer gives us confidence in our ability to achieve the next experimental goal: characterization of confined nanoscale structures in which the discrete electronic spectrum has energy-level spacings in the terahertz regime.

ACKNOWLEDGMENTS

This research was supported by the Laboratory Directed Research and Development Program of Lawrence Berkeley Laboratory under U.S. Department of Energy contract DE-AC03-76ST00098. C. Karadi was supported in part by a graduate fellowship from the U.S. Department of Education, S. Jauhar was supported in part by a graduate fellowship from the National Science Foundation, L. P. Kouwenhoven was supported by a fellowship from the Royal Netherlands Academy of Arts and Sciences, and P. L. McEuen was supported in part by the Alfred P. Sloan Foundation and the Packard Foundation.

*Also with Quantum Wave Project, ERATO, Research Development Corporation of Japan.

REFERENCES AND NOTES

1. Q. Hu, Appl. Phys. Lett. **62,** 837 (1993); S. Feng and Q. Hu, Phys. Rev. B **48,** 5354 (1993).
2. N. S. Wingreen, A.-P. Jauho, and Y. Meir, Phys. Rev. B **48,** 8487 (1993).
3. S. Datta and M. P. Anatram, Phys. Rev. B **45,** 13,761 (1992).
4. F. Hekking and Y. V. Nazarov, Phys. Rev. B **44,** 11506 (1991).
5. T. Brandes, W. Hausler, K. Jauregui, B. Kramer, and D. Weinmann, Physica B **189,** 16 (1993).
6. M. Buttiker, A. Pretre, and H. Thomas, Phys. Rev. Lett. **70,** 4114 (1993).
7. Y. Fu and S. C. Dudley, Phys. Rev. Lett. **70,** 65 (1993).
8. L. P. Kouwenhoven, S. Jauhar, K. McCormick, D. Dixon, P. L. McEuen, Y. V. Nazarov, N. C. van der Vaart, and C. T. Foxon, "Photon-assisted tunneling through a quantum dot," Phys. Rev. B **50,** 2019 (1994).
9. B. J. van Wees, H. van Houten, C. W. J. Beenakker, J. G. Williamson, L. P. Kouwenhoven, D. van der Marel, and C. T. Foxon, Phys. Rev. Lett. **60,** 848 (1988).
10. D. A. Wharam, T. J. Thornton, R. Newbury, M. Pepper, H. Ahmed, J. E. F. Frost, D. G. Hasko, D. C. Peacock, D. A. Ritchie, and G. A. C. Jones, J. Phys. C **21,** L209 (1988).
11. N. K. Patel, T. J. B. M. Janssen, J. Singleton, M. Pepper, G. A. C. Jones, J. E. F. Frost, D. A. Ritchie, D. C. Peacock, R. J. Brown, H. Ahmed, D. G. Hasko, and J. A. A. J. Perenboom, in *Proceedings of the Twentieth International Conference on the Physics of Semiconductors*, E. M. Anastassakis and J. D. Joannopoulos, eds. (World Scientific, Singapore, 1990), Vol. 3, p. 2371.
12. R. A. Wyss, C. C. Eugster, J. A. del Alamo, and Q. Hu, Appl. Phys. Lett. **63,** 1522 (1993).
13. B. I. Greene, J. F. Federici, D. R. Dykaar, R. R. Jones, and P. H. Bucksbaum, Appl. Phys. Lett. **59,** 893 (1991).
14. C. Karadi, S. Verghese, C. A. Mears, J. Orenstein, P. L. Richards, and A. T. Barfknecht, in *OSA Proceedings on Ultrafast Electronics and Optoelectronics*, J. Shah and U. Mishra, eds. (Optical Society of America, Washington, D.C., 1993), Vol. 14, p. 231; S. Verghese, C. Karadi, C. A. Mears, J. Orenstein, P. L. Richards, and A. T. Barfknecht, Appl. Phys. Lett. **64,** 915 (1994).
15. D. H. Auston, in *Ultrashort Laser Pulses: Generation and Applications*, Vol. 60 of Topics in Applied Physics, 2nd ed., W. Kaiser, ed. (Springer-Verlag, New York, 1992), pp. 183–233.
16. M. van Exter and D. Grischkowsky, IEEE Trans. Microwave Theory Technol. **38,** 1684 (1991).
17. Y. Nagamune, H. Sakaki, L. P. Kouwenhoven, L. C. Mur, C. J. P. M. Harmans, J. Motohisa, and H. Noge, Appl. Phys. Lett. **64,** 2379 (1994).
18. R. Landauer, IBM J. Res. Dev. **32,** 306 (1988).
19. Y. Imry, in *Directions in Condensed Matter Physics*, G. Grinstein and G. Mazenko, eds. (World Scientific, Singapore, 1986), p. 101.
20. M. Buttiker, Phys. Rev. Lett. **57,** 1761 (1986).
21. A proportionality factor of 100 is chosen so that the calculated conductance has a threshold near $V_g = -700$ mV $= -100E_f/e$.
22. P. N. Butcher and D. Cotter, *The Elements of Nonlinear Optics* (Cambridge University Press, Cambridge, UK, 1990), p. 16.
23. P. R. Griffiths and J. A. deHaseth, *Fourier Transform Infrared Spectrometry* (Wiley, New York, 1986), p. 15.
24. P. K. Tien and J. P. Gordon, Phys. Rev. **129,** 647 (1963).